Transition from Optically Excited to Intrinsic Spin Polarization in WSe_2

S. Hedwig,[1] G. Zinke,[1] J. Braun,[2] B. Arnoldi,[1] A. Pulkkinen,[3] J. Minár,[3] H. Ebert,[2] M. Aeschlimann,[1,*] and B. Stadtmüller[4,†]

[1]*Department of Physics and Research Center OPTIMAS, Rheinland-Pfälzische Technische Universität Kaiserslautern-Landau, 67663 Kaiserslautern, Germany*

[2]*Department Chemie, Physical Chemistry, Ludwig-Maximilians-Universität München, 81377 München, Germany*

[3]*New Technologies Research Centre, University of West Bohemia, 301 00 Plzeň, Czech Republic*

[4]*Experimentalphysik II, Institute of Physics, University of Augsburg, 86159 Augsburg, Germany*

(Received 3 June 2025; accepted 6 October 2025; published 31 October 2025)

Layered 2D van der Waals materials, such as transition metal dichalcogenides, are promising for nanoscale spintronic and optoelectronic applications. Harnessing their full potential requires understanding both intrinsic transport and the dynamics of optically excited spin and charge carriers, particularly the transition between excited spin polarization and the conduction band's intrinsic spin texture. Here, we investigate the spin polarization of the conduction bands of bulk WSe_2 using static and time-resolved spin-resolved photoemission spectroscopy, complemented by photocurrent calculations. Electron doping reveals the intrinsic spin polarization, while time-resolved measurements trace the evolution of excited spin carriers. We find that intervalley scattering is spin-conserving, with spin transport initially governed by photoexcited carriers and aligning with the intrinsic conduction band spin polarization after ∼150 fs.

DOI: 10.1103/lc2p-kl4y

Transition metal dichalcogenides have emerged as a prominent class of two-dimensional materials with remarkable electronic, optical, and spintronic properties, making them attractive for both fundamental research and technological applications [1–4]. Among these materials, WSe_2 has garnered significant attention due to its unique spin-related phenomena, including large spin-orbit coupling (SOC) and valley-dependent spin properties, which arise from its broken inversion symmetry and strong SOC in the transition metal atoms. As a bulk crystal, WSe_2 exhibits an indirect band gap between the valence band maximum at K/K′ and the Σ valley of the conduction band, whereas the monolayer features a direct band gap at the K and K′ points [5]. Importantly, the strong SOC in both monolayer and bulk WSe_2 induces substantial spin splitting, particularly in the valence band, creating spin polarization locked to specific valleys (K and K′), a phenomenon known as spin-valley coupling [6,7]. Combined with local symmetry breaking, this leads to highly spin-polarized bands that globally compensate due to inversion symmetry, resulting in a Kramers degenerate spin polarization across the Brillouin zone, an effect called "hidden spin polarization" [8,9]. This enables spin functionalities without magnetization, offering potential for future low-power spin-based technologies [10]. While the valence band spin properties of bulk WSe_2 have been extensively studied [9,11–13], the spin texture of the conduction band remains largely unexplored [14]. Only recently was the spin polarization of excitons directly measured in a photoemission experiment [15]. However, excitonic spin polarization does not necessarily reflect the intrinsic spin polarization of the conduction band, which governs electronic charge transport in such materials. Optically excited populations undergo various scattering processes leading to energy and spin relaxation and redistribution in momentum space, thus defining carrier transport on a microscopic level. An important question in the framework of optoelectronic and spintronic applications is how ultrafast spin polarization of excited carriers relates to the intrinsic spin polarization of the transport states. Equally important is the transition between these regimes, reflecting the transition from ballistic to diffusive transport. A previous Letter tracked the spin polarization decay of photoexcited bright excitons at the K and K′ points using time- and spin-resolved angle-resolved photoemission spectroscopy (ARPES) [15]. Interestingly, the authors observed a time-independent spin-down polarization of intervalley scattered excitons at the Σ valley, independent of the excitation light helicity, highlighting their potential as local spin reservoirs for spin injection in transition metal dichalcogenide heterostructures. However, they did not observe any temporal transition at the Σ valleys from the

*Contact author: ma@physik.uni-kl.de

†Contact author: benjamin.stadtmueller@uni-a.de

initially excited to the steady scattered ensemble spin polarization.

In this Letter, we aim to shed new light on the spin polarization of the conduction band of bulk WSe_2. In particular, we compare the intrinsic single-particle spin polarization of the conduction band and the optically excited spin carrier dynamics and their respective relaxation timescales. Recent advances in experimental techniques, such as time- and spin-resolved pump-probe photoemission spectroscopy, offer a powerful approach to directly probe the spin texture and dynamics in the conduction band. These techniques enable time-resolved mapping of spin polarization in momentum space, allowing deeper insights into ultrafast spin relaxation mechanisms and spin-dependent scattering processes in WSe_2. In combination with static spin-resolved measurements performed on alkali-metal doped WSe_2 and photoemission calculations, this allows us to directly access and disentangle the intrinsic and optically excited spin polarization of conduction band electrons.

We start with the single-particle spin polarization of the conduction band, defining the diffusive transport properties. We first compare the calculated spin-resolved photoemission intensity and the band structure obtained in static spin-resolved photoemission experiments on an alkali-metal doped WSe_2 crystal. The performed photocurrent calculations (see "Methods" below for further details) take into account final state effects, enhancing comparison with the experimental data. Figure 1 depicts the calculated photoemission intensity (a) and the corresponding out-of-plane (P_z) component of the calculated spin polarization (b) for a photoemission process with $h\nu = 21$ eV along the $\Gamma - \mathrm{K}$ direction of a bulk WSe_2 crystal. The energy axis is referenced to the maximum of the valence band, which shows a strong spin-orbit splitting of (0.48 ± 0.04) eV at the K and K′ points around $k_{\parallel} = \pm(1.28 \pm 0.02)$ Å^{-1}, which is, as well as the overall band dispersion, in very good agreement with previous experimental findings and density-functional theory calculations [9,16–18]. As expected from time reversal symmetry, the spin polarization is inverted at the K and K′ points. The local conduction band minima at the K and K′ points also exhibit a considerable spin splitting of (80 ± 4) meV and follow the spin sequence of the valence bands. At the Σ points at $k_{\parallel} = \pm(0.69 \pm 0.02)$ Å^{-1}, the conduction band shows a global minimum at $E - E_{\mathrm{VBmax}} = (1.05 \pm 0.02)$ eV and a spin polarization opposite to that of the lower conduction band branch at the respective K point. This energy also marks the electronic transport gap of the calculated band structure.

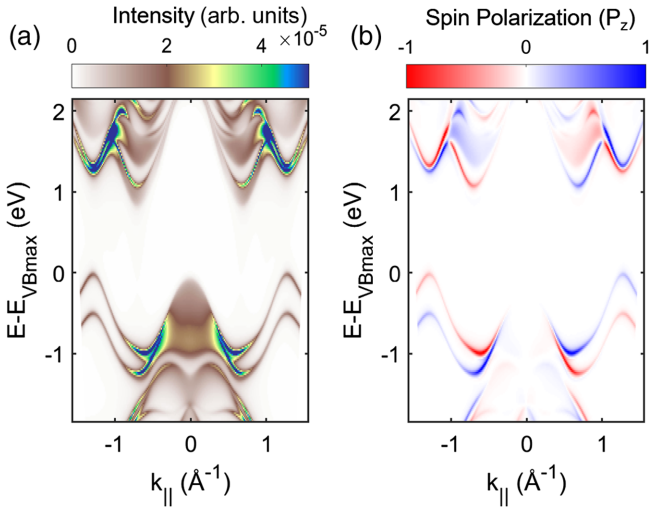

FIG. 1. Calculated photoemission spectra of bulk WSe_2 along the $\Gamma - \mathrm{K}$ direction. (a) Spin-integrated intensity and (b) out-of-plane spin polarization P_z, with blue (red) marking spin-up (spin-down) spin polarization. The energy axis is referenced to the valence band maximum.

To experimentally access the single-particle spin polarization of the conduction band at the high-symmetry K and Σ points, we performed static spin-resolved ARPES measurements on a potassium-doped WSe_2 sample. The doping results in an electron transfer from the alkali metal to the WSe_2 semiconductor, raising the chemical potential and ultimately populating the conduction band. A discussion of the changes in the ARPES spectrum upon potassium doping and further characterization of the doped band structure is found in the End Matter.

Figures 2(a) and 2(b) show the measured spin-resolved photoemission signal at the conduction band onset at the

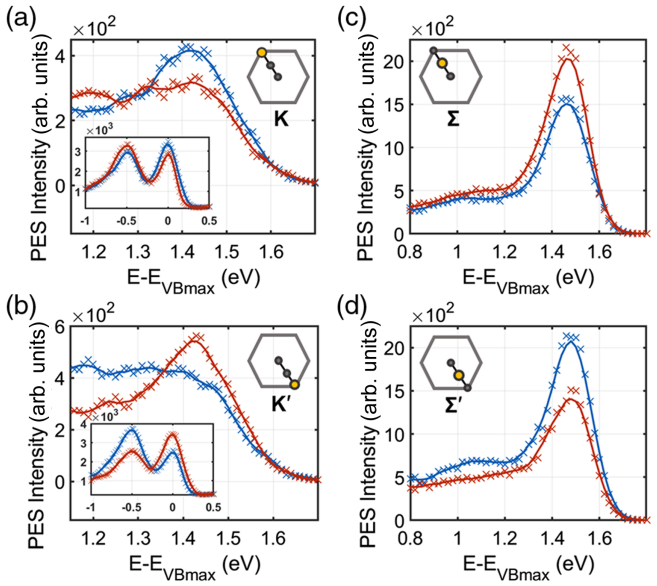

FIG. 2. (a),(b) Spin-resolved spectra of the conduction band of potassium doped WSe_2 at the K (a) and K′ point (b) of the Brillouin zone (sketch in the corner of each graph). The corresponding valence band spectra are shown as insets. (c), (d) Spin-resolved spectra of the conduction band at the Σ (c) and the Σ′ (d) point. Blue (red) markers refer to the measured spin-up (spin-down) data points, the same-colored solid lines represent the smoothed signal for better visualization.

K and K′ points, respectively, with valence band spectra as insets for reference. The spin polarization at the Σ and Σ′ points is shown in Figs. 2(c) and 2(d). All spectra were obtained for an electron concentration of 4.6×10^{13} cm^{-2}, resulting from potassium doping of the WSe_2 surface, as discussed in the End Matter. Blue (red) markers represent measured spin-up (spin-down) signal, and solid lines show the smoothed signal. The different symmetry points are visualized within a sketch of the hexagonal surface Brillouin zone in the corner of each plot. With the used photon energy of 21.2 eV, the photoelectrons have a rather small inelastic mean free path of ∼1 nm in WSe_2, so that mainly the first two (tri)layers contribute to the measured spin signal with a ratio of around 3:1 between first and second layers [9,19,20].

It can be seen that the spin polarization of the conduction band at the K points [Figs. 2(a) and 2(b)] follows that of the upper valence bands and is positive at the K point and negative at the K′ point. The conduction band at the Σ and Σ′ points [Figs. 3(c) and 3(d)] also shows an opposing spin polarization, which is negative at the Σ point and positive at the Σ′ point, opposite to the spin polarization observed at the corresponding K points. Overall, the spin polarization of the valence and conduction band at the four measured symmetry points shows the alternating behavior in its sign, as expected from time reversal symmetry.

To compare the findings for the intrinsic spin polarization with those of excited spin carrier populations, we conducted time-, spin-, and angle-resolved pump-probe photoemission experiments. This enables complementary access to the conduction band of WSe_2 and allows one to probe the ultrafast spin polarization dynamics after optical excitation. In particular, electrons in the valence band are optically excited into previously unoccupied conduction states at the K point, using an ultrashort circularly polarized near-infrared laser pulse (< 40 fs, 1.59 eV). The evolution of the excited system is then probed by a second time-delayed ultrashort extreme ultraviolet (XUV) probe pulse (< 30 fs, 22.3 eV [21]), ultimately photoemitting the excited charge carriers. With applied pump fluencies up to 6.2 mJ/cm^2, lying in an excitation regime well above the critical Mott density where a transition between exciton gas and electron-hole plasma takes place [22,23], we expect to excite mostly free carriers in the conduction band rather than excitons. By using left (σ^-) and right (σ^+) circularly polarized pump pulses, spin-up or spin-down carriers at the K points can be selectively excited into the conduction band [7,14,24–26]. The measurements were conducted at identical momentum-space positions $\tilde{\mathbf{K}}$ and $\tilde{\mathbf{\Sigma}}$ (i.e., identical emission angles of the photoelectrons) along the $\Gamma - \mathrm{K}$ direction with varying pump light polarization, as illustrated in Figs. 3(a) and 3(b). Because of the high surface sensitivity of the XUV probe light, the combined photoemission signal of only the first (L1) and second (L2) layer is obtained, as mentioned before. Along the observed $\Gamma - \mathrm{K}$ direction, this means that with σ^--polarized pump light, all K points in the first and second layers are excited but the signal is mainly obtained from the first layer, whereas for σ^+-polarized pulses, all K′ points of the first two layers are addressed but the measured signal stems mostly from the second layer. The probed momentum-space regions within the surface Brillouin zone are highlighted in green in Figs. 3(a) and 3(b) and are labeled as $\tilde{\mathbf{K}}$ and $\tilde{\mathbf{\Sigma}}$, in order to distinguish them from the inequivalent

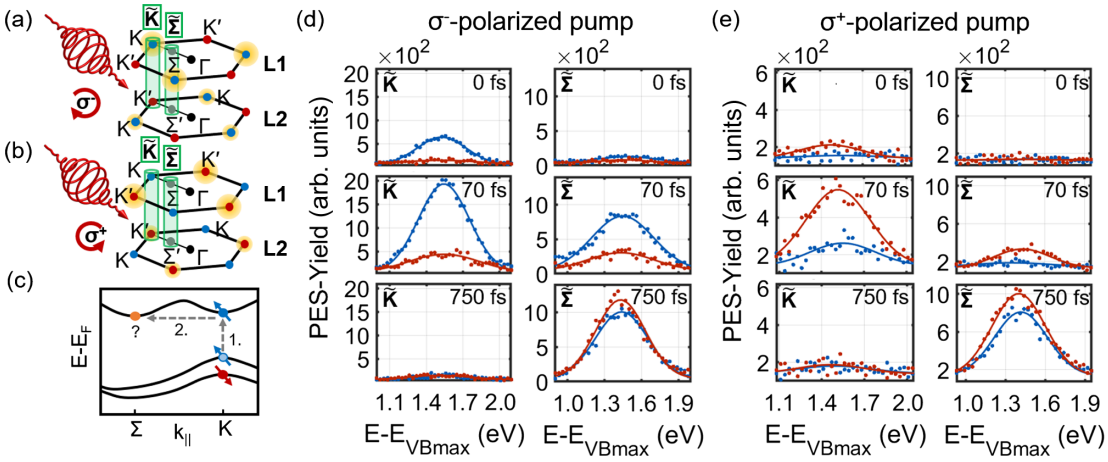

FIG. 3. Sketch of the hexagonal surface Brillouin zone of the first (L1) and second (L2) layer of WSe_2 for excitation with σ^- (a) and σ^+-polarized (b) pump pulses. Depending on pump helicity, spin carriers are excited at different points, indicated by yellow coronas. Their size reflects the layer-dependent contribution to the signal. Measurements were performed at the same fixed $\tilde{\mathbf{K}}$ and $\tilde{\mathbf{\Sigma}}$ positions marked in green, either exciting the K point of L1 (σ^--light) or the K′ of L2 (σ^+-light). (c) Excitation scheme: (1) spin-selective excitation of carriers from the valence to conduction band at the K point; (2) intervalley scattering to the Σ point. (d),(e) Spin-up (blue) and spin-down (red) photoemission intensities and Gaussian fits at 0, 70, and 750 fs after σ^- (d) and σ^+ (e) excitation. Left and right columns show signals at the $\tilde{\mathbf{K}}$ and $\tilde{\mathbf{\Sigma}}$ points, respectively.

high-symmetry points K/K′ and Σ/Σ′. The light polarization and layer-dependent contribution to the photoemission signal is illustrated by a yellow corona around the excited K/K′ points. Figure 3(c) depicts the excitation scheme for an exemplary excitation with σ^--polarized light. Upon selective optical excitation of spin carriers from the valence band to the conduction band at the K point (1.), a subsequent intervalley scattering process from the K to the Σ point takes place (2.). One important goal here is to elucidate the spin polarization and its evolution, especially after scattering to the Σ point, to gain insight into the relaxation of the nonequilibrium spin population. Known mechanisms that lead to depolarization of the valleys include intervalley exchange coupling between neighboring K and K′ points, whereby both electron and hole are transferred, individually flipping their spin [27–30], as well as phonon-mediated relaxation processes [31–33]. In the following, we discuss the results for the conduction band. Corresponding time- and spin-resolved measurements of the valence band, which reflect the hole dynamics, are presented in Fig. S1 in Supplemental Material (SM) [34]. Figure 3(d) shows the measured spin signal at the K point of the conduction band in the left column and the Σ point in the right column for three time steps (0, 70, and 750 fs) after optical excitation with σ^--polarized light. Blue (red) dots represent the measured spin-up (spin-down) data points, whereas the lines of the same color are corresponding Gaussian fits. Note that the absolute intensities of the spectra in the different columns cannot be directly compared as they were acquired in separate time-resolved photoemission experiments. At 0 fs, marking the onset of the excitation, a ∼75% spin-up polarized population at the K point can be observed, while no significant population has yet scattered to the Σ point. At 70 fs later, the population at the K point has exceeded its maximum with still ∼70% spin-up polarization. The small amount of spin-down electrons observed in the signal most likely stems from a combination of spin-flip scattered and backscattered carriers due to intervalley exchange coupling between the K and K′ point, as well as an imperfect light polarization, leading to an additional weak excitation of spin-down carriers at the K′ points of the second layer. At the same time (70 fs), a population of the same spin-up polarization is found at the Σ point. This indicates that the initial scattering from the K to the Σ point is spin-conserving. At 750 fs after optical excitation, nearly all excited carriers at the K point have either recombined or scattered to the neighboring valley at the Σ point. Remarkably, the population at the Σ point shows a complete reversal of the sign of spin polarization at 750 fs after the initial excitation, with a surplus of spin-down carriers.

The same experiment was repeated with σ^+-polarized light. In this case, mainly the K′ point of the second layer in the observed region is excited. The results are shown in Fig. 3(e). After a spin-selective excitation of spin-down carriers at the K′ point of the second layer, the initial scattering toward the Σ′ valley again proves to be spin-preserving, confirming the observation made with σ^--polarized excitation in Fig. 3(d). At 750 fs after optical excitation, no change in the sign of the spin polarization is observed at the Σ′ point. Instead, a finite spin-down polarization is present, similar to that observed for σ^--polarized excitation in Figs. 3(d) and 3(c) indicating that this corresponds to the intrinsic spin polarization at the Σ valley. The same spin-down polarization has recently also been reported for scattered dark excitons at the Σ valley following initial excitation at the K point with σ^-- and σ^+-polarized light [15]. However, in that Letter, no thermalization of the scattered spin carriers was observed; instead, a time-independent spin-down polarization persisted. We further conducted additional time- and spin-resolved measurements at the Σ′ point of the first layer after excitation with σ^--polarized light (see Fig. S2 in SM [34]). On longer timescales (750 fs) after optical excitation, the scattered population exhibits a clear spin-up polarization. This is in very good agreement with the intrinsic spin polarizations at the Σ and Σ′ valley of the conduction band observed on potassium-doped WSe_2, shown in Figs. 2(c) and 2(d). This consistency between the two complementary approaches allows the spin polarization of the scattered population on longer timescales to be directly related to the intrinsic single-particle spin polarization of the conduction band. The equalization of the spin polarization can further be associated with carrier thermalization at the Σ point, as observed in additional spin-integrated and highly time-resolved measurements (see Fig. S3 in SM [34]), enabling a classification of the relevant time scales.

In conclusion, our time-, spin-, and angle-resolved photoemission experiments provide insight into the nature of the spin polarization at the conduction band valleys of WSe_2 as well as the evolution of optically excited nonequilibrium spin populations. After a spin-selective initial excitation of spin carriers at the K points, depending on the pump light helicity, the subsequent intervalley scattering to the Σ points appears to be spin-conserving. For later times after the scattering, a finite spin-down (spin-up) polarization is observed at the Σ (Σ′) valley, which is independent from the initially excited and scattered spin carriers. This hints at an SOC mediated and spin-flip involving thermalization of the scattered nonequilibrium populations at the Σ points and an equalization of the spin polarization due to interaction of neighboring Σ points, as suggested in previous Letter [14]. Comparing these findings with the spin polarization of potassium-doped WSe_2, it can be seen that in both cases the spin polarization exhibits the same behavior with a finite spin polarization at the respective Σ points of the conduction band. As a result, this indicates an equalization of the optically excited and initially spin-conserved scattered spin carriers at the Σ valleys toward the intrinsic spin polarization of the conduction band. For spin

transport in optoelectronic or spintronic applications, this means that on short timescales ($\lesssim$150 fs) the spin state of excited spin carriers is preserved even after phonon-mediated intervalley scattering. This is particularly important for spin-conserving ballistic transport processes at interfaces, where the optically excited carriers thus define the spin properties of the system, which do not necessarily reflect the intrinsic spin polarization of the material they enter. The latter becomes important at longer times ($\lesssim$150 fs), when the excited spin carriers have equilibrated to the intrinsic spin polarization via spin relaxation processes. For diffusive transport involving frequent scattering events, the essential spin characteristics are therefore governed by the intrinsic single-particle spin polarization of the material.

Methods—All photoemission experiments were performed at room temperature under UHV conditions ($\sim 10^{-10}$ mbar) using a hemispherical energy analyzer (SPECS Phoibos 150) in combination with a CCD detector for ARPES and a commercial VLEED spin filter system (Focus FERRUM) [41] for 1D spin-resolved measurements. The spin-resolved data were taken for the out-of-plane spin component. As light sources, we used the He Iα line (21.2 eV) of a monochromatic He gas discharge lamp (Scienta VUV5k) for static measurements and a high harmonic generation setup providing linearly polarized fs-pulsed XUV radiation (< 30 fs, 22.3 eV) for the time-resolved experiments. For the high harmonic generation process, the frequency doubled (390 nm) output of a Ti:Sa laser amplifier system (780 nm, 10 kHz, < 40 fs) is used [21]. The fundamental of the amplifier system (1.59 eV) is used for the optical excitation of the sample in a pump-probe interferometric scheme. The spatial overlap of the pump and probe beam was optimized directly on the sample before each experiment and was actively stabilized during the measurements. The pump light helicity can be selected using an additional quarter wavelength plate in the beam path.

The 2H-WSe_2 samples were purchased from HQ graphene and were cleaved *in situ* under UHV conditions to obtain a flat and clean surface. Furthermore, potassium doping was achieved by *in situ* evaporation from a commercial alkali-metal dispenser onto the WSe_2 surface under UHV conditions. The doping level was controlled by the evaporation time and verified via the observed shifts in the valence band spectra. In addition to our experimental data, we conducted self-consistent electronic structure calculations within the *ab initio* framework of density-functional theory. For these calculations, we employed the Vosko *et al.* parametrization to account for the exchange and correlation potential [42]. The electronic structure was determined in a fully relativistic mode by solving the Dirac equation, utilizing the relativistic multiple-scattering formalism, also known as the Korringa-Kohn-Rostoker method, in the full potential Korringa-Kohn-Rostoker mode [43–45].

Photocurrent calculations were based on the resulting half-space electronic structure, which was represented by single-site scattering matrices for the various layers. These matrices, along with the wave functions corresponding to the initial and final state energies, were used as input quantities.

Acknowledgments—The experimental work was funded by the Deutsche Forschungsgemeinschaft (DFG, German Research Foundation)—TRR 173–268565370 Spin + X: spin in its collective environment (Projects A02). J. M. and A. P. thank the project Quantum Materials for applications in sustainable technologies (QM4ST), funded as Project No. CZ.02.01.01/00/22_008/0004572 by Programme Johannes Amos Comenius, call Excellent Research.

Data availability—The data that support the findings of this article are not publicly available upon publication because it is not technically feasible and/or the cost of preparing, depositing, and hosting the data would be prohibitive within the terms of this research project. The data are available from the authors upon reasonable request.

[1] Z. Yin, H. Li, H. Li, L. Jiang, Y. Shi, Y. Sun, G. Lu, Q. Zhang, X. Chen, and H. Zhang, ACS Nano **6**, 74 (2012).
[2] S. Ding, D. Zhang, J. S. Chen, and X. W. Lou, Nanoscale **4**, 95 (2012).
[3] B. Radisavljevic and A. Kis, Nat. Mater. **12**, 815 (2013).
[4] Q. H. Wang, K. Kalantar-Zadeh, A. Kis, J. N. Coleman, and M. S. Strano, Nat. Nanotechnol. **7**, 699 (2012).
[5] K. F. Mak, C. Lee, J. Hone, J Shan, and T. F. Heinz, Phys. Rev. Lett. **105**, 136805 (2010).
[6] Z. Y. Zhu and U. Schwingenschlögl, Phys. Rev. B **84**, 153402 (2011).
[7] D. Xiao, G.-B. Liu, W. Feng. X. Xu and W. Yao, Phys. Rev. Lett. **108**, 196802 (2012).
[8] X. Zhang, Q. Liu, J.-W. Luo, A. J. Freeman, and A. Zunger, Nat. Phys. **10**, 387 (2014).
[9] J. Riley *et al.*, Nat. Phys. **10**, 835 (2014).
[10] E. C. Ahn, npj 2D Mater. Appl. **4**, 17 (2020).
[11] S.-K. Mo, C. Hwang, Y. Zhang, M. Fanciulli, S. Muff, J. H. Dil, Z.-X. Shen, and Z. Hussain, J. Phys. Condens. Matter **28**, 454001 (2016).
[12] M. Gehlmann *et al.*, Sci. Rep. **6**, 26197 (2016).
[13] E. Razzoli *et al.*, Phys. Rev. Lett. **118**, 086402 (2017).
[14] R. Bertoni *et al.*, Phys. Rev. Lett. **117**, 277201 (2016).
[15] M. Fanciulli *et al.*, Phys. Rev. Lett. **131**, 066402 (2023).
[16] T. Finteis *et al.*, Phys. Rev. B **55**, 10400 (1997).
[17] Traving M. *et al.*, Phys. Rev. B **55**, 16 (1997).
[18] D. Voß, P. Krüger, A. Mazur, and J. Pollmann, Phys. Rev. B **60**, 14311 (1999).
[19] B. Parashar *et al.*, Phys. Rev. Mater. **7**, 044004 (2023).
[20] B. Arnoldi, S. L. Zachritz, S. Hedwig, M. Aeschlimann, O. L. A. Monti, and B. Stadtmüller, Nat. Commun. **15**, 3573 (2024).
[21] S. Eich *et al.*, J. Electron Spectrosc. Relat. Phenom. **195**, 231 (2014).

[22] M. Puppin, Ph.D. thesis, FU Berlin, 2017 available online at https://refubium.fu-berlin.de/handle/fub188/23006.
[23] A. Chernikov, C. Ruppert, H. M. Hill, A. F. Rigosi, and T. F. Heinz, Nat. Photonics **9**, 466 (2015).
[24] K. F. Mak, K. He, J. Shan, and T. F. Heinz, Nat. Nanotechnol. **7**, 494 (2012).
[25] H. Zeng, J. Dai, W. Yao, D. Xiao, and X. Cui, Nat. Nanotechnol. **7**, 490 (2012).
[26] T. Cao *et al.*, Nat. Commun. **3**, 887 (2012).
[27] M. Z. Maialle, E. A. de Andrada e Silva, and L. J. Sham, Phys. Rev. B **47**, 15776 (1993).
[28] T. Yu and M. W. Wu, Phys. Rev. B **89**, 205303 (2014).
[29] R. Schmidt, G. Berghäuser, R. Schneider, M. Selig, P. Tonndorf, E. Malic, A. Knorr, S. Michaelis de Vasconcellos, and R. Bratschitsch, Nano Lett. **16**, 2945 (2016).
[30] M. Selig, F. Katsch, S. Brem, G. F. Mkrtchian, E. Malic, and A. Knorr, Phys. Rev. Res. **2**, 023322 (2020).
[31] M. Selig, G. Berghäuser, A. Raja, P. Nagler, C. Schüller, T. F. Heinz, T. Korn, A. Chernikov, E. Malic, and A. Knorr, Nat. Commun. **7**, 13279 (2016).
[32] A. Molina-Sánchez, D. Sangalli, L. Wirtz, and A. Marini, Nano Lett. **17**, 4549 (2017).
[33] Z. Wang *et al.*, Nano Lett. **18**, 6882 (2018).
[34] See Supplemental Material at http://link.aps.org/supplemental/10.1103/lc2p-kl4y for additional data on the spin-resolved valence band and hole dynamics, a comparison of the scattered spin polarization at the Σ and Σ′ points, and the thermalization of excited carrier populations, which includes Refs. [35–40].
[35] S. Dong *et al.*, Nat. Sci. **1**, e10010 (2021).
[36] R.-Y. Liu *et al.*, Sci. Rep. **7**, 15981 (2017).
[37] U. De Giovanni, H. Hübener, and A. Rubio, Nano Lett. **16**, 12 (2016).
[38] S. Aeschlimann *et al.*, Nano Lett. **21**, 12 (2021).
[39] M. Schüler and S. Beaulieu, Commun. Phys. **5**, 164 (2022).
[40] R. Wallauer, J. Reimann, N. Armbrust, J. Güdde, and U. Höfer, Appl. Phys. Lett. **109**, 162102 (2016).
[41] M. Escher, N. B. Weber, M. Merkel, L. Plucinski, and C. M. Schneider, J. Surf. Sci. Nanotechnol. **9**, 340 (2011).
[42] S. H. Vosko, L. Wilk, and M. Nusair, Can. J. Phys. **58**, 1200 (1980).
[43] H. Ebert *et al.*, The Munich SPR-KKR package, version 8.5, https://www.ebert.cup.uni-muenchen.de/en/software-en/13-sprkkr (2020).
[44] H. Ebert, D. Ködderitzsch, and J. Minár, Rep. Prog. Phys. **74**, 096501 (2011).
[45] H. Ebert, in *Electronic Structure and Physical Properties of Solids*, edited by H. Dreyssé, (Springer, Berlin, Heidelberg, 2000).
[46] B. S. Kim, J.-W. Rhim, B. Kim, C. Kim, and S. R. Park, Sci. Rep. **6**, 36389 (2016).
[47] T. Komesu *et al.*, Appl. Phys. Lett. **105**, 241602 (2014).
[48] Y. Zhang *et al.*, Nano Lett. **16**, 2485 (2016).
[49] T. Eknapakul *et al.*, Nano Lett. **14**, 1312 (2014).
[50] J. Park *et al.*, J. Phys. Chem. C **129**, 5065 (2025).

End Matter

Potassium doping of the WSe_2 *surface*—In order to experimentally access the single-particle spin polarization of the conduction band at the high-symmetry K points and the corresponding Σ points between Γ and K, we performed static spin-resolved measurements on a potassium-doped system. The doping process results in an electron transfer from the alkali metal to the WSe_2 semiconductor, which increases the chemical potential and ultimately populates the WSe_2 conduction band for sufficiently high doping concentrations. We start by discussing the change in the experimentally obtained ARPES spectrum upon potassium doping. First of all, Figs. 4(a)–4(c) show the static momentum-resolved photoemission intensity along the $\Sigma - K$ direction around the Fermi level for pristine WSe_2 (a) and for two exemplary steps of potassium doping with e^- doping concentrations of 2.2×10^{13} cm^{-2} (b) and 4.6×10^{13} cm^{-2} (c). The electron doping concentrations have been estimated in accordance with [46]. The photoemission yield is plotted logarithmically to better visualize the band dispersion of the populated conduction band alongside the much more intense valence bands. With successive potassium doping, the valence bands shift to larger binding energies $E_B = -(E - E_F)$ which in Figs. 4(b) and 4(c) is indicated by the black and red dashed lines related to the valence band maximum at the K point in Fig. 4(a). The energetic position of the valence band maximum with respect to the Fermi level E_F for different potassium doping steps is depicted in Fig. 4(d), showing an initial strong shift to larger binding energies that asymptotically approaches a constant energy position with an increasing amount of doping as the surface gets more and more saturated with potassium. The valence band maximum at the K point shifts from $E - E_F = (-1.27 \pm 0.02)$ eV for undoped WSe_2 [Fig. 4(a)] to $E - E_F = (-1.54 \pm 0.02)$ eV for the highest amount of potassium doping [Fig. 4(c)], resulting in an overall energy shift of the valence band maximum of $\Delta E = (-0.27 \pm 0.02)$ eV. With consecutive potassium doping, the chemical potential is lifted above the onset of the conduction band at the Σ point, leading to a population of the previously unoccupied conduction band minimum, now lying below the Fermi energy E_F, as can be seen in Fig. 4(b).

For the highest amount of potassium doping also, the onset of the local conduction band minimum at the K point is weakly populated [see right side in Fig. 4(c)]. Besides that, additional dispersive features arise below the conduction band, which are addressed to adsorbate states

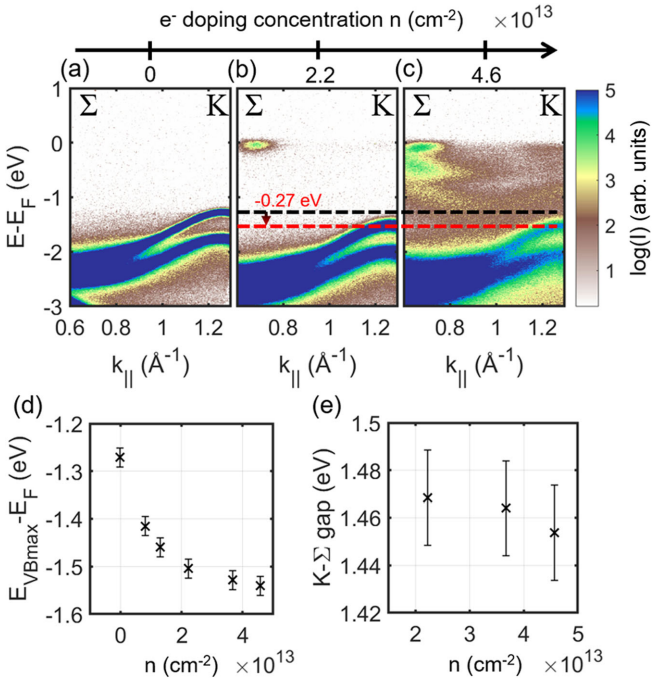

FIG. 4. (a)–(c) ARPES maps of the band structure of bulk WSe_2 along the $\Sigma - K$ direction for the pristine crystal (a) and two exemplary steps of potassium doping with e^- doping concentrations of 2.2×10^{13} cm^{-2} (b) and 4.6×10^{13} cm^{-2} (c). From the undoped system to the highest amount of potassium doping, the valence band maximum shifts by -0.27 eV, which is indicated by the dashed black and red lines. (d) Shift of the valence band maximum at the K point with increasing potassium doping with respect to the Fermi level. (e) Size of the band gap between the valence band maximum at the K point and the conduction band minimum at the Σ point.

resulting from the increased potassium doping at the surface. As shown in Fig. 4(e), the size of the indirect $K - \Sigma$ band gap (measured between the intensity peak maxima) is slightly reduced to $E_g = (1.45 \pm 0.02)$ eV at the highest potassium doping concentration, suggesting a larger shift of the conduction band compared to the valence band. Such band structure renormalizations upon alkali-metal doping have been observed before [46–48]. However, the change is comparable to the experimental uncertainty and should be interpreted qualitatively. At the K point, the weak conduction band intensity appears at $E - E_F = (-0.12 \pm 0.02)$ eV, corresponding to $E_K - E_{VBmax} = (1.42 \pm 0.02)$ eV relative to the valence band maximum. While this spectral intensity is located close to the conduction band minimum at Σ ($E_\Sigma - E_{VBmax} = 1.45 \pm 0.02$ eV), the low spectral weight indicates that only the onset of the conduction band at the K point, cut by the high energy cutoff of the Fermi-Dirac distribution, is observed rather than its actual intensity maximum. The center of mass of the spectral weight of the conduction band likely resides above E_F. Consequently, the exact energetic position of the conduction band valley at the K point remains ambiguous, and our data do not provide evidence for a transition from an indirect to a direct band gap. Moreover, the presence of adsorbate-related states suggests that potassium predominantly remains on the surface rather than intercalating into the van der Waals gap, as observed in [49,50], making the formation of a quasifreestanding monolayer unlikely. Nevertheless, the observed reduction of the energetic separation between the K and Σ valleys suggests a general tendency of the electronic structure to evolve toward a more monolayerlike character under increasing surface doping.